Journal of Statistical Physics, Vol. 110, Nos. 3–6, March 2003 (© 2003)

Phase Separation of Penetrable Core Mixtures

R. Finken,[1] J.-P. Hansen,[1] and A. A. Louis[1]

Received October 8, 2001; accepted November 16, 2001

A two-component system of penetrable particles interacting via a gaussian core potential is considered, which may serve as a crude model for binary polymer solutions. The pair structure and thermodynamic properties are calculated within the random phase approximation (RPA) and the hypernetted chain (HNC) integral equation. The analytical RPA predictions are in semi-quantitative agreement with the numerical solutions of the HNC approximation, which itself is very accurate for gaussian core systems. A fluid-fluid phase separation is predicted to occur for a broad range of potential parameters. The pair structure exhibits a nontrivial clustering behaviour of the minority component. Similiar conclusions hold for the related model of parabolic core mixtures, which is frequently used in dissipative particle dynamics (DPD) simulations.

KEY WORDS: Gaussian core potential; phase separation; random phase approximation.

1. INTRODUCTION

Demixing of binary or multicomponent mixtures is a very common phenomenon observed in a broad range of molecular fluids,[1] polymer solutions and blends,[2,3] or colloidal dispersions.[4,5] Phase separation is generally associated with differences in the attractive interactions between particles of different chemical species. In polymer solutions these differences are usually embodied in the Flory χ-parameter,[2] which controls the competition between the entropy of mixing and the total interaction energy, at least within a mean-field picture. On the other hand, in multicomponent colloidal systems like binary dispersions involving colloidal particles of very different sizes, or mixtures of colloidal particles and nonadsorbing polymer, phase separation can be driven by purely repulsive, excluded volume interactions. By mapping the initial multi-component

[1] Department of Chemistry, University of Cambridge, Cambridge CB2 1EW, United Kingdom; e-mail: rf227@cam.ac.uk

0022-4715/03/0300-1015/0 © 2003 Plenum Publishing Corporation

system onto an *effective* one-component system involving only the bigger colloidal particles, the largely entropy-driven demixing can be understood in terms of *attractive* depletion interactions induced between the large particles by the smaller species (the "depletant").[5] It should however be kept in mind that the initial bare interactions are purely repulsive, albeit strongly non-additive, as in the highly simplified Asakura–Oosawa model for colloid-polymer mixtures.[6] In the case of fully additive hard sphere mixtures, phase separation has been predicted for sufficiently large size ratios,[7] but it is now generally believed that the fluid-fluid demixing is metastable, and preempted by freezing.[8] A significant degree of positive non-additivity of the core radii $R_{\mu\nu}$ (whereby $R_{12} = (R_{11} + R_{22})(1 + \Delta)/2$, with $\Delta > 0$) is required to observe a stable demixing transition in the fluid phase.[9]

Effective interactions between the centres of mass of fractal objects, like linear polymer coils,[10–13] star polymers[14] or dendrimers,[15] obtained by averaging over individual monomer degrees of freedom, are now known to be very "soft." More specifically the effective pair potential diverges only logarithmically for overlapping star polymers,[14] while remaining finite, of the order of $1 - 2k_BT$, for linear polymers in good solvent.[10–13] This observation has stimulated the investigation of simple models, like finite repulsive step potentials,[16] or the gaussian core potential,[17–19] which was first introduced by Stillinger, in a somewhat different context,[20] namely

$$v(r) = \epsilon \exp(-r^2/R^2), \tag{1}$$

where ϵ is the energy scale, while R determines the range of the effective potential. It is worth stressing that the "gaussian core" model is unrelated to the "gaussian molecule" model, which was extensively studied by Michael Fisher and collaborators.[21] In the latter model it is the Mayer f-function, rather than the pair potential, which has a gaussian shape.

Simple, penetrable particle models are also widely used in highly coarse-grained simulations of large-scale phenomena within the so-called "dissipative particle dynamics" (DPD) method.[22, 23] In DPD, effective interactions between penetrable fluid "particles" are frequently modelled by a simple parabolic potential:[23, 24]

$$v(r) = \begin{cases} \epsilon(1 - r/R)^2; & r < R \\ 0; & r \geqslant R. \end{cases} \tag{2}$$

It has recently been realized that binary mixtures of particles with penetrable cores, which interact via generalizations of the gaussian and parabolic

potentials (1) and (2), involving different energy scales ϵ and radii R for the various species, may phase-separate over appropriate ranges of these parameters. Spinodal instability was first shown to occur for the gaussian core model (1) within the random phase approximation (RPA)[18] and binodals as well as interfacial properties were then calculated within the same approximation.[19] Similarly Gibbs ensemble Monte Carlo simulations have very recently shown that binary systems of soft particles interacting via the parabolic potential (2) phase separate beyond a critical degree of enhanced repulsion between particles of different species, in agreement with Flory-like mean field considerations.[24]

In this paper we systematically extend our earlier results for the gaussian core model[18] and investigate the range of validity of the RPA by detailed calculations of the pair structure, thermodynamics, and the resulting phase coexistence curve within the much more accurate hypernetted chain (HNC) approximation. The break-down of the RPA is quantified in the physically relevant regime where $\rho R^3 \simeq 1$ and $\epsilon \simeq k_B T$, which would correspond to the cross-over from dilute to semi-dilute regimes of the underlying binary polymer solution. The RPA continues to provide reliable first estimates at higher densities.

2. RPA AND HNC

The model under consideration is the binary gaussian core model (GCM) already introduced in refs. 18 and 19. It consists of N_1 particles of "radius" R_1 and N_2 particles of "radius" R_2 in a volume V. The total number density is $\rho = (N_1 + N_2)/V$, while the concentrations of the two species are $x = N_2/N$ and $1-x = N_1/N$, respectively. The pair potentials are

$$v_{\mu\nu}(r) = \epsilon_{\mu\nu} e^{-(r/R_{\mu\nu})^2}, \tag{3}$$

which introduce three length and three energy parameters: R_{11}, R_{22}, R_{12}, ϵ_{11}, ϵ_{12} and ϵ_{22}. If R_{11} is chosen as unit of length, the system is entirely specified by the 5 dimensionless parameters R_{12}/R_{11}, R_{22}/R_{11}, $\epsilon_{11}^* = \beta\epsilon_{11}$, $\epsilon_{12}^* = \beta\epsilon_{12}$, $\epsilon_{22}^* = \beta\epsilon_{22}$, where $\beta = 1/(k_B T)$. For a fixed set of dimensionless parameters the reduced Helmholtz free energy per particle, $f = F/(N k_B T)$, is a function only of the intensive variables ρ and x; this may be split into the ideal gas, ideal mixing and excess (non-ideal) contributions:

$$f(\rho, x) = f_{\text{id}}(\rho) + f_{\text{mix}}(x) + f_{\text{ex}}(\rho, x) \tag{4a}$$

$$= \ln(\rho \Lambda^3) - 1 + x \ln x + (1-x)\ln(1-x) + f_{\text{ex}}(x, \rho), \tag{4b}$$

where Λ is an irrelevant de Broglie thermal wavelength. The equation of state $\beta P/\rho$, and the chemical potentials μ_ν, $(\nu = 1, 2)$ follow from the standard thermodynamic relations:

$$\frac{\beta P}{\rho} = \rho \left(\frac{\partial f}{\partial \rho}\right)_x \tag{5a}$$

$$\beta\mu_1 = \left(\frac{\partial \rho f}{\partial \rho}\right)_x - x\left(\frac{\partial f}{\partial x}\right)_\rho \tag{5b}$$

$$\beta\mu_2 = \left(\frac{\partial \rho f}{\partial \rho}\right)_x + (1-x)\left(\frac{\partial f}{\partial x}\right)_\rho \tag{5c}$$

and may likewise be split into ideal and excess contributions. Within RPA and HNC, these excess contributions may be easily expressed in terms of the usual total and direct correlation functions $h_{\mu\nu}(r)$ and $c_{\mu\nu}(r)$, which are related by the familiar Ornstein–Zernike (OZ) relations;[25] these may be used to express the Fourier transforms (FT) $\hat{h}_{\mu\nu}(k)$ of the total correlation functions in terms of the FT $\hat{c}_{\mu\nu}(k)$ of the direct correlation functions:

$$\hat{h}_{11}(k) = \frac{1}{\Delta(k)}\left[\hat{c}_{11}(k)(1-\rho_2\hat{c}_{22}(k)) + \rho_2\hat{c}_{12}^2(k)\right], \tag{6a}$$

$$\hat{h}_{12}(k) = \frac{1}{\Delta(k)}\,\hat{c}_{12}(k), \tag{6b}$$

$$\hat{h}_{22}(k) = \frac{1}{\Delta(k)}\left[\hat{c}_{22}(k)(1-\rho_1\hat{c}_{11}(k)) + \rho_1\hat{c}_{12}^2(k)\right], \tag{6c}$$

where $\rho_1 = \rho(1-x)$, $\rho_2 = \rho x$, and

$$\Delta(k) = [1-\rho_1\hat{c}_{11}(k)][1-\rho_2\hat{c}_{22}(k)] - \rho_1\rho_2\hat{c}_{12}^2(k). \tag{7}$$

These OZ relations must be supplemented by closure relations.

The RPA amounts to simply identifying the $c_{\mu\nu}(r)$ with their asymptotic (large r) behaviour:

$$\begin{aligned} c_{\mu\nu}(r) &= -\beta v_{\mu\nu}(r) \\ &= -\epsilon^*_{\mu\nu} e^{-(r/R_{\mu\nu})^2} \end{aligned} \tag{8}$$

Substitution of the FT's of (8) into the relations (6) and (7) yields explicit expressions for the $\hat{h}_{\mu\nu}(k)$, which may be transformed back to obtain the $h_{\mu\nu}(r)$. Detailed analytical expressions are given in Appendix A in the special case of mixtures with equal core radii $R_{11} = R_{22} = R_{12} = R$.

The HNC closure relations are:[25]

$$g_{\mu\nu}(r) = 1 + h_{\mu\nu}(r)$$
$$= \exp\{-\beta v_{\mu\nu}(r) + \gamma_{\mu\nu}(r)\} \tag{9a}$$
$$\gamma_{\mu\nu}(r) = h_{\mu\nu}(r) - c_{\mu\nu}(r) \tag{9b}$$

An iterative procedure must be used to solve the coupled Eqs. (6) and (9) numerically. Convergence is easily achieved for the binary GCM model over most of the potential parameter space. In fact the HNC approximation becomes exact in the high density limit ($\rho R^3 \to \infty$), and is extremely accurate for densities $\rho R^3 \approx 1$, as shown earlier in the one-component case.[17, 18] Pair structure data will be examined in greater detail in Section 5.

Knowledge of the pair correlation functions allows direct access to thermodynamics, via the compressibility or virial routes.[25] Being approximate, the RPA and HNC closures are not thermodynamically consistent, i.e., the two routes lead to different answers. In the case of the GCM the two theories become strictly thermodynamically consistent only in the high density limit.[17, 18]

Within the RPA, the compressibility route is equivalent to a simple mean-field ansatz for the free energy.[17, 18] This leads immediately to the following analytic expression for the excess part of the reduced free energy:[18]

$$f_{\text{ex}}^{\text{C}}(x, \rho) = \tfrac{1}{2}\rho V_0(x) \tag{10a}$$
$$= \tfrac{1}{2}\rho \sum_{\nu} \sum_{\mu} x_\mu x_\nu V_{\mu\nu} \tag{10b}$$
$$V_{\mu\nu} = \beta \hat{v}_{\mu\nu}(k=0) = \int \beta v_{\mu\nu}(r)\, d\mathbf{r}, \tag{10c}$$

where $x_1 = (1-x)$, $x_2 = x$. In the special case of the GCM:

$$V_{\mu\nu} = \pi^{3/2} \epsilon^*_{\mu\nu} R^3_{\mu\nu} \tag{11}$$

The pressure and chemical potentials μ_ν follow directly from Eqs. (5) (the superscript C refers to the compressibility route):

$$\frac{\beta P^{\text{C}}}{\rho} = 1 + \frac{\rho}{2} \sum_{\mu} \sum_{\nu} x_\mu x_\nu V_{\mu\nu} \tag{12a}$$
$$\beta\mu_1^{\text{C}} = \ln(\rho\Lambda^3(1-x)) + V_{11}\rho(1-x) + V_{12}\rho x \tag{12b}$$
$$\beta\mu_2^{\text{C}} = \ln(\rho\Lambda^3 x) + V_{12}\rho(1-x) + V_{22}\rho x \tag{12c}$$

The virial route is considerably more arduous. The pressure follows from the virial theorem:

$$\frac{\beta P^{\mathrm{V}}}{\rho} = 1 + \frac{\rho}{2} \sum_{\mu} \sum_{\nu} x_\mu x_\nu V_{\mu\nu} - \frac{2\pi}{3} \rho \sum_{\mu} \sum_{\nu} x_\mu x_\nu \int_0^\infty r^3 \frac{d\beta v_{\mu\nu}(r)}{dr} h_{\mu\nu}(r)\, dr \tag{13}$$

In the case of the symmetric mixture ($R_{11} = R_{22} = R_{12} = R$; $V_{11} = V_{22}$) the RPA pair correlation functions obtained in Appendix A may be used to yield the following expression (the superscript V referring to the virial route):

$$\frac{\beta P^{\mathrm{V}}}{\rho} = \frac{\beta P^{\mathrm{C}}}{\rho} - \frac{z_2 x(1-x)\, \Delta}{\pi^{3/2} R^3} \aleph\left(-\frac{\rho}{z_1}\right) - \frac{z_1 x(1-x)\, \Delta}{\pi^{3/2} R^3} \aleph\left(-\frac{\rho}{z_2}\right), \tag{14}$$

where the functions $\aleph(s)$ and the roots z_1 and z_2 are defined in Appendix A (Eqs. (A4a) and (A4b)). The resulting reduced free energy per particle is obtained by integrating the equation of state (14) with respect to density:

$$f^{\mathrm{V}}(x, \rho) = f^{\mathrm{C}}(x, \rho) + \frac{1}{2\pi^{3/2} \rho R^3} [\mathrm{Li}_{5/2}(\rho/z_1) + \mathrm{Li}_{5/2}(\rho/z_2) + \rho V_{11}], \tag{15}$$

where the polylogarithm $\mathrm{Li}_{5/2}$ is defined in equation (A7). Unfortunately this expression becomes singular for densities larger than the spinodal densities obtained by the compressibility route. This mathematical artifact discussed in Appendix A does not allow us to use expressions (14) and (15) to construct a phase diagram.

The lack of thermodynamic consistency of the RPA is illustrated in Fig. 1, which compares the compressibility and virial equations of state as a function of density, for a symmetric mixture; the virial pressures are always lower than their compressibility counterparts, and closer to the nearly exact HNC results, to which we now turn.

The HNC approximation is very nearly thermodynamically consistent in practice, at least for temperatures and densities relevant for polymer solutions.[18] Hence we have calculated thermodynamic properties within the more convenient virial route with the pressure given by the standard

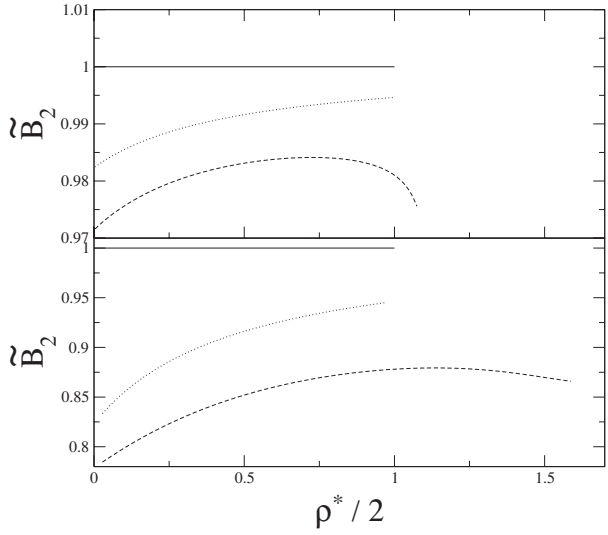

Fig. 1. The normalised effective second virial coefficient $\tilde{B}_2 = 4(\beta P - \rho)/(3\rho^2 V_{11})$ is plotted versus the normalized density $\rho^*/2$ at fixed concentration $x = 0.5$ for RPA-C, RPA-V and HNC. In the upper plot, we have $\epsilon_{11}^* = \epsilon_{22}^* = 0.1, \epsilon_{12}^* = 0.2$, while in the lower plot $\epsilon_{11}^* = \epsilon_{22}^* = 1.0, \epsilon_{12}^* = 2.0$. Both systems have the reduced critical density $\rho_c^* = 2$ in RPA-C. The RPA-C route predicts $\tilde{B}_2 = 1$ at all densities (solid line). The RPA-V values are represented by the dotted lines, the HNC data by the dashed lines up to the density beyond which convergence fails. The agreement between the three routes to the equation of state is seen to improve with increasing density, except in the vincinity of the critical density where the results diverge again.

relation (13), while the chemical potentials may also be directly expressed in terms of the direct and total correlation functions, according to:[26]

$$\beta\mu_\nu = \ln(\rho_\nu \Lambda^3) + \sum_\mu \left\{ \frac{\rho_\mu}{2} \int d\mathbf{r}\, h_{\nu\mu}(r)[h_{\nu\mu}(r) - c_{\nu\mu}(r)] - \rho_\mu \hat{c}_{\nu\mu}(k=0) \right\}. \qquad (16)$$

Note that these expressions hold only within the HNC approximation, and are consistent with the virial route (13).

3. SCALING PROPERTIES

As mentioned earlier, suitably reduced equilibrium properties of the binary GCM depend on the five dimensionless combinations R_{12}/R_{11}, R_{22}/R_{11}, ϵ_{11}^*, ϵ_{12}^*, and ϵ_{22}^*. The compressibility version of the RPA thermodynamics (or equivalently, the mean field approximation) allows a considerable reduction of this parameter space. From the expressions (10)–(12c) it

is clear that the radii $R_{\mu\nu}$ and energies $\epsilon_{\mu\nu}$ enter only in the combinations $V_{\mu\nu}$ defined in Eq. (11). In terms of the reduced density $\rho^* = \rho V_{11}$ and pressure $P^* = \beta P V_{11}$, the thermodynamic behaviour of the mixture is uniquely determined by the dimensionless ratios V_{22}/V_{11} and $V_{12}/\sqrt{V_{11}V_{22}}$. This remarkable reduction of parameter space holds only for the thermodynamics, but not for the correlation functions, which depend explicitly on the five parameters of the GCM potentials. The scale invariance of the thermodynamics is broken by the RPA virial route, as is immediately evident form the explicit expressions (14) and (15) (valid for a symmetric mixture); the same is true within the HNC approximation.

However deviations from RPA-C (mean-field) scale invariance are expected to be small in the high density, high temperature regime, where RPA is increasingly accurate, so that the considerable reduction in the number of relevant potential parameters (from 5 to 2) is expected to carry over, at least approximately, to the phase diagrams calculated with RPA-V or HNC thermodynamics, which will be presented in the next section.

4. PHASE DIAGRAMS

The phase behaviour of the binary GCM may be deduced from the knowledge of the reduced free energy per particle f as a function of the variables $v = 1/\rho$ and x and from its thermodynamic derivatives (the pressure and the chemical potentials). For suitable values of the potential parameters $\epsilon_{\mu\nu}$ and $R_{\mu\nu}$, the binary GCM becomes unstable against demixing at sufficiently high densities. In terms of the free energy per particle, $f = f(v, x)$, the standard thermodynamic stability conditions of a binary mixture read:[1]

$$\left(\frac{\partial^2 f}{\partial v^2}\right)_x > 0; \qquad \left(\frac{\partial^2 f}{\partial x^2}\right)_v > 0 \tag{17a}$$

$$\left(\frac{\partial^2 f}{\partial v^2}\right)_x \left(\frac{\partial^2 f}{\partial x^2}\right)_v - \left(\frac{\partial^2 f}{\partial v \partial x}\right)^2 > 0. \tag{17b}$$

The first condition ensures mechanical stability, while the second inequality guarantees stability against demixing at constant volume; the third inequality ensures stability of the mixture at constant pressure. Note that the stability at constant pressure is the more restrictive condition.

The subsequent discussion is restricted to demixing at constant pressure. The vanishing of the l.h.s. of Eq. (17b), corresponding to the case where the third inequality turns into an equality, signals the occurrence of

spinodal instability. Within the mean-field (RPA-C) approximation (10), the equation for the spinodal is easily calculated to be[18]

$$1+\rho V_1(x)-\rho^2 x(1-x)\,\Delta V=0, \tag{18}$$

where:

$$V_1(x)=(1-x)\,V_{11}+xV_{22} \tag{19a}$$

$$\Delta V=V_{12}^2-V_{11}V_{22}. \tag{19b}$$

It is easily inferred from (18) that a spinodal instability occurs whenever $V_{12}/\sqrt{V_{11}V_{22}}>1$. This region is visualized in Fig. 2 in a plot of the minimum energy ratio $\epsilon_{12}/\sqrt{\epsilon_{11}\epsilon_{22}}$ required for spinodal instability, as a function of the size ratio R_{22}/R_{11}. The radius R_{12} is taken to be given by the combination rule:

$$R_{12}^2=\tfrac{1}{2}\,(R_{11}^2+R_{22}^2), \tag{20}$$

as suggested by renormalization group (RG) calculations[11] and by direct simulation[12] of mixtures of self-avoiding polymer coils.

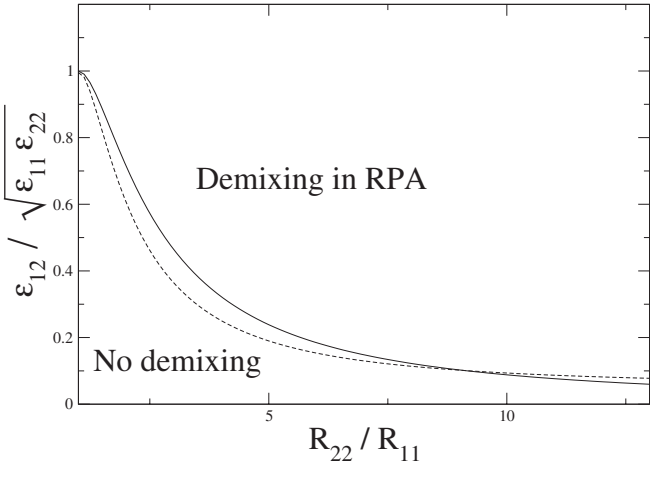

Fig. 2. Mixing/demixing regions within RPA-C, in the $\epsilon_{12}/\sqrt{\epsilon_{11}\epsilon_{22}}$ vs. R_{22}/R_{11} plane. Above the solid line phase separation is predicted by RPA-C. Corresponding values of $\epsilon_{12}/\sqrt{\epsilon_{11}\epsilon_{22}}$ predicted for polymers with radii of gyration R_{11} and R_{22} by a renormalisation group theory of Krüger *et al.*[11] are plotted as the dashed curve. The intersection of these curves at $R_{22}/R_{11}\approx 10$ suggests the possibility of a phase separation in polymer mixtures with extreme size ratios.

Figure 2 also shows the values of the ratio $\epsilon_{12}/\sqrt{\epsilon_{11}\epsilon_{22}}$, as calculated for two self-avoiding walk polymers by RG techniques,[11] plotted as a function of the ratio of their radii of gyration. The figure suggests that phase separation of real polymers would only be observed for ratios of gyration radii larger than 10, i.e., for mixtures of very long and very short polymers. However, the RG results are probably not trustworthy for such asymmetric mixtures, and the RG potentials are strictly valid only in the infinite dilution limit.

The spinodal line in the $P-x$-plane is easily calculated from (18) to be:

$$\rho_S(x) = \frac{V_1(x) + \sqrt{[V_1(x)]^2 + 4x(1-x)\,\Delta V}}{2x(1-x)\,\Delta V} \tag{21}$$

The critical concentration is determined by the condition:

$$\frac{dP_S(x)}{dx} = 0, \tag{22}$$

where $P_S(x)$ is the pressure calculated from (12a), at the spinodal density given by (21). The corresponding critical density ρ_C, calculated by substituting the critical concentration determined by (22) is plotted in Fig. 3 versus the ratio $V_{12}/\sqrt{V_{11}V_{22}}$, for several ratios V_{22}/V_{11}.

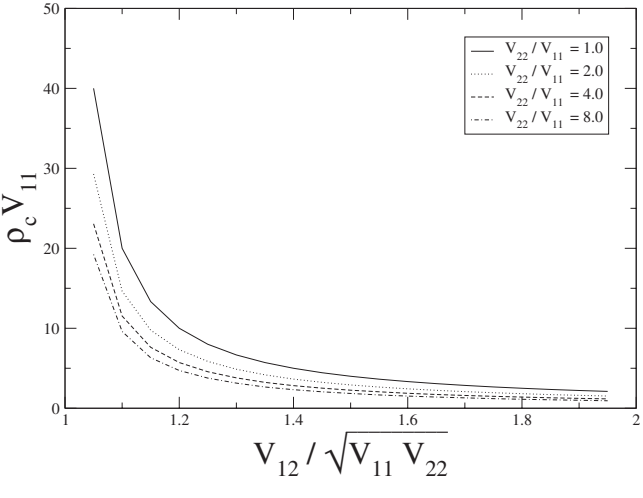

Fig. 3. Reduced critical densities $\rho_c V_{11}$ vs. $V_{12}/\sqrt{V_{11}V_{22}}$, for several values of V_{22}/V_{11} from RPA-C (shown in the inset).

The binodal or phase coexistence curves in the $\rho - x$ plane are determined by the usual conditions of equality of the chemical potentials of both species and of the pressures in the two phases, using expressions (12a)–(12c). The resulting equations must in general be solved numerically to yield the binodal curves. The complete phase diagram can however be calculated analytically within the RPA-C approximation, in the symmetric case, where $V_{11} = V_{22}$. Due to the symmetry of the problem, all thermodynamic quantities must be invariant with respect to the transformation $1 \leftrightarrow 2$; $x \leftrightarrow (1-x)$ and $\rho \leftrightarrow \rho$. This simplification allows the fully analytic treatment detailed in Appendix B. The resulting spinodal and binodal are shown in Fig. 4 in the case where $V_{12}/V_{11} = 2$. The same figure also shows the HNC binodals, for several values of ϵ_{11}^* (remember that within RPA-C all these binodals coincide). As expected the HNC results break the scale invariance of RPA-C and shift the binodal curves upward, to higher densities. The HNC and RPA-C critical densities differ by almost a factor of 2 for $\epsilon_{11}^* = 2$, pointing to the limitations of the mean-field (RPA-C) description.

An example of a phase diagram in an asymmetric mixture, with potential parameters already used in earlier RPA calculations,[18, 19] is shown in Fig. 5 in the $\rho - x$ plane and in Fig. 6 in the $P - x$ plane. The spinodal and binodal curves are now asymmetric, and the difference

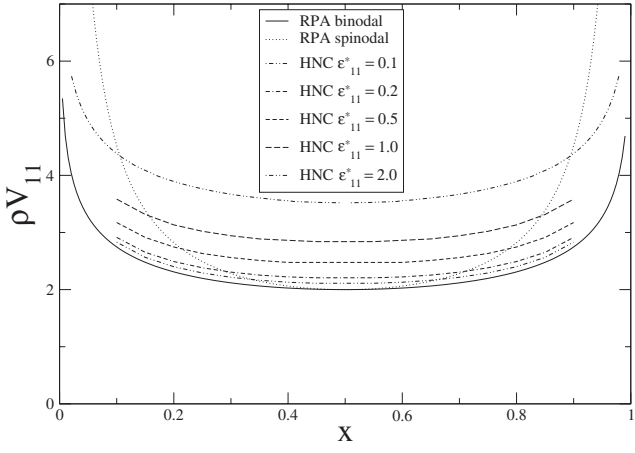

Fig. 4. Binodal for a symmetric GCM mixture with $V_{12}/V_{22} = 2$ for values of $\epsilon_{11}^* = \epsilon_{22}^* = 0.2, 0.5, 1.0, 2.0$, determined by RPA-C (full curves) and HNC (dashed curve). The RPA-C binodal and spinodal (dotted line) depend only on the ratio V_{12}/V_{11}. The HNC binodal does not obey the same scale invariance and is shifted to higher reduced density as ϵ_{11} increases.

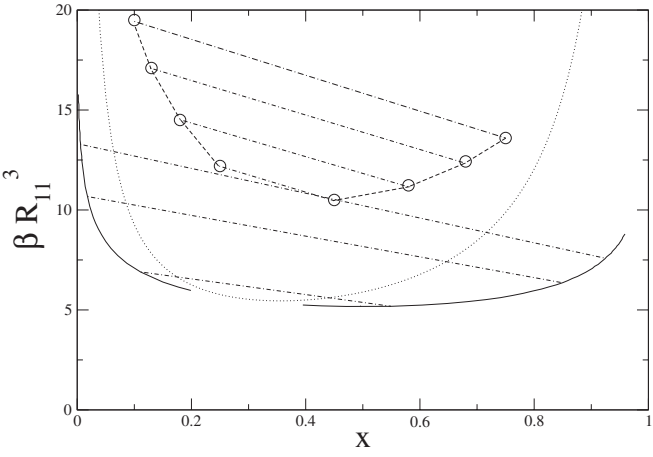

Fig. 5. Phase diagram in ρ-x plane for asymmetric mixture with $R_{11} = 1$, $R_{12} = 0.665$, $R_{22} = 0.849$, $\epsilon_{11}^* = \epsilon_{22}^* = 2$, $\epsilon_{12}^* = 1.888$. The solid curve is the RPA-C binodal with examples of tie-lines of coexisting phases as dash-dotted lines. The dotted line is the RPA spinodal. The circles and dashed curve represent the HNC binodal with tie-lines shown again as dash-dotted lines.

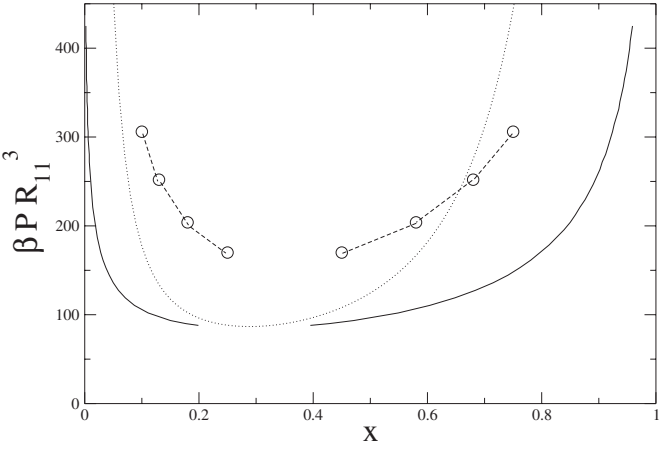

Fig. 6. Phase diagram in P-x plane for asymmetric mixture with $R_{11} = 1$, $R_{12} = 0.665$ and $R_{22} = 0.849$, $\epsilon_{11}^* = \epsilon_{22}^* = 2$, $\epsilon_{12}^* = 1.888$. Symbols as in Fig. 5. The tie-lines in this plot (not shown) are horizontal.

between RPA-C and HNC results is again significant, with the HNC binodal being pushed to higher densities.

Phase separation in binary mixtures of particles interacting via the closely related parabolic core potentials (2) has been observed in the Gibbs ensemble Monte Carlo simulations of Wijmans *et al.*[24] They considered the symmetric case where all $R_{\mu\nu}$ are equal, $\epsilon^*_{11} = \epsilon^*_{22}$ and $\epsilon^*_{12} = \epsilon^*_{11} + \Delta\epsilon^*$. We have calculated the binodal in the $\Delta\epsilon^* - x$ plane under the same conditions as the MC simulations, i.e., for $\epsilon^*_{11} = 12.5$, $\rho^*_b = \rho_b R^3 = 3$, in the RPA and HNC approximations. The results are compared to the MC data in Fig. 7. In view of the fact that the amplitude of the parabolic repulsion is $12.5 k_B T$, which makes it more hard-core like, the agreement may be considered to be rather satisfactory. As in the GCM case, the HNC coexistence-curve lies well above its RPA counterpart; it is closer to the simulation data.

5. PAIR STRUCTURE AND CLUSTERING

The pair correlation functions $h_{\mu\nu}(r)$ of the GCM mixture can be calculated by combining the OZ relations (6) with either the RPA closure (8)

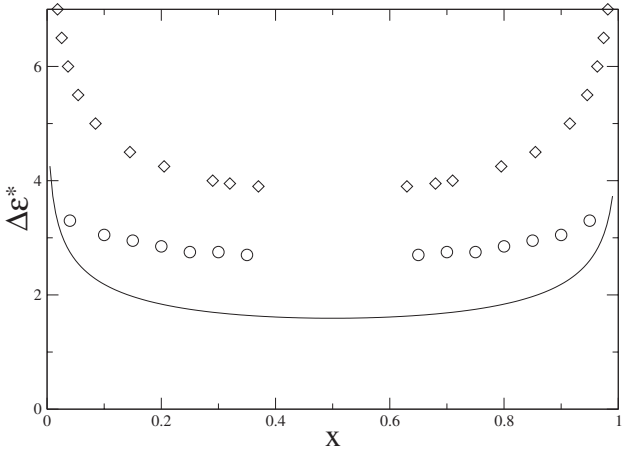

Fig. 7. Binodal of the parabolic core system (2) investigated by Wijmans *et al.*[24] Here $\epsilon^*_{11} = \epsilon^*_{22} = 12.5$ is kept fixed and ϵ^*_{12} is determined so that the binodal density has the fixed value $\rho_b R^3 = 3.0$ at any given concentration x. The required difference $\Delta\epsilon^* = \epsilon^*_{12} - \epsilon^*_{11}$ is plotted vs. x. Note that in ref. 24 twice that value is plotted due to a different definition of the potential parameters. The diamonds correspond to the simulation data of Wijmans *et al.*,[24] the solid line represents the RPA-C prediction. The HNC results are plotted as circles. While RPA-C underestimates the required ϵ^*_{12} for the given binodal density by a factor of two, the HNC results lie closer to the simulation data, although a significant discrepancy remains. This may be due to the high amplitude ϵ^*_{12} of the potentials, making the particles more hard-sphere like.

or the HNC closure (9). In the symmetric case, characterized by a single gaussian range parameter $R_{11} = R_{22} = R_{12} = R$, analytic expressions, in the form of infinite series, can be obtained for the RPA closure, as shown in Appendix A. In the asymmetric case, solutions for the $h_{\mu\nu}(r)$ are readily obtained by numerical Fourier transformation of Eq. (6) and (7), using the straightforward Fourier transforms of the $c_{\mu\nu}(r)$ given by (8).

The HNC closure requires an iterative solution of the coupled OZ and closure equations. This was achieved using the standard Picard method, and well-converged solutions were generally obtained in a few iterations. Convergence was found to be slower in the vicinity of phase coexistence, and to break down rapidly inside the phase coexistence region corresponding to metastable mixtures. Concentration fluctuations build up in that region, as signalled by a $k = 0$ peak of growing amplitude in the $\hat{h}_{\mu\nu}(k)$, or equivalently in the corresponding partial structure factors

$$S_{\mu\nu}(k) = x_\mu \delta_{\mu\nu} + x_\mu x_\nu \rho \hat{h}_{\mu\nu}(k) \tag{23}$$

The concentration-concentration structure factor:

$$S_{CC}(k) = x_2^2 S_{11}(k) - 2x_1 x_2 S_{12}(k) + x_1^2 S_{22}(k) \tag{24}$$

satisfies the long wavelength limit:[25]

$$\lim_{k \to 0} S_{CC}(k) = \frac{N k_B T}{(\partial^2 G / \partial x^2)_{N,P,T}}, \tag{25}$$

where G is the Gibbs free energy. The cross-over from metastable to unstable mixture corresponds to the vanishing of $(\partial^2 G/\partial x^2)_{N,P,T}$, so that $S_{CC}(k = 0)$ is expected to diverge along a spinodal line.

This is indeed the case with the RPA closure, but the HNC closure ceases to converge before a spinodal line is reached, a well-known shortcoming of the HNC closure.[27] Such a break-down is typical of the inadequacy of fluid integral equations to describe critical behaviour.[28] The accuracy of HNC in the stable one-phase region for the pair correlation function $h(r)$, already documented in the one-component GCM,[17,18] is tested under more severe conditions (namely $\epsilon^* = 12.5$) in Fig. 8 against recent Monte Carlo data[24] for the parabolic core potential (2). The agreement is seen to be excellent. This suggests that the HNC closure would be very useful to generate pair structure in coarse-grained DPD fluids at a moderate computational cost.

Examples of pair correlation functions and partial structure factors for several states of GCM mixtures are shown in Figs. 9–11. The most striking feature is the amount of structure observed both in r and in k-space, even

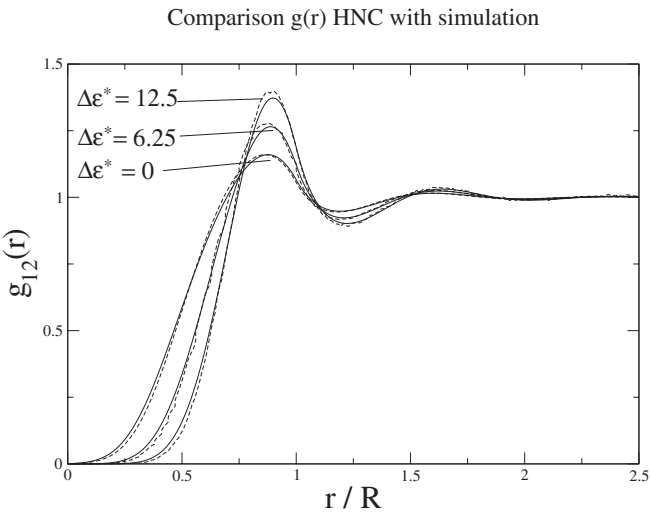

Fig. 8. A comparison between HNC predictions for $g_{12}(r)$ and the simulation data of Wijmans *et al.* for the parabolic potential (2) with $\epsilon^*_{11} = \epsilon^*_{22} = 12.5$. The potential amplitude between unlike partikles ϵ^*_{12} is varied as $\epsilon^*_{12} = \epsilon^*_{11} + \Delta\epsilon^*$ with $\Delta\epsilon^* = 0$, 6.25, 12.5. The simulation data are plotted as dashed lines, while HNC results are plotted as solid lines. Note that $g_{12}(r \to 0)$ is very near zero, in contrast to the case of the much softer potentials studied in ref. 18 and the subsequent figures.

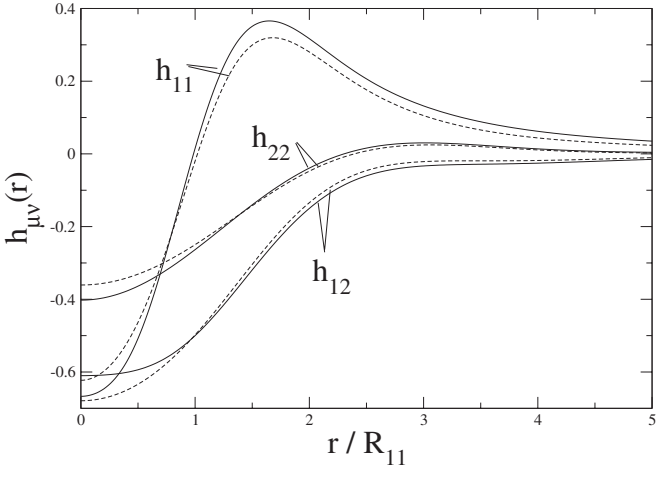

Fig. 9. Pair correlation function $h_{\mu\nu}(r)$ for the non-symmetric system $R_{11} = 1.0$, $R_{12} = 1.582$, $R_{22} = 2.0$, $\epsilon^*_{11} = \epsilon^*_{12} = \epsilon^*_{22} = 2.0$, $\rho R^3_{11} = 0.188$, $x = 0.5$. The solid lines represent the RPA results, while HNC correlation functions are the dashed curves.

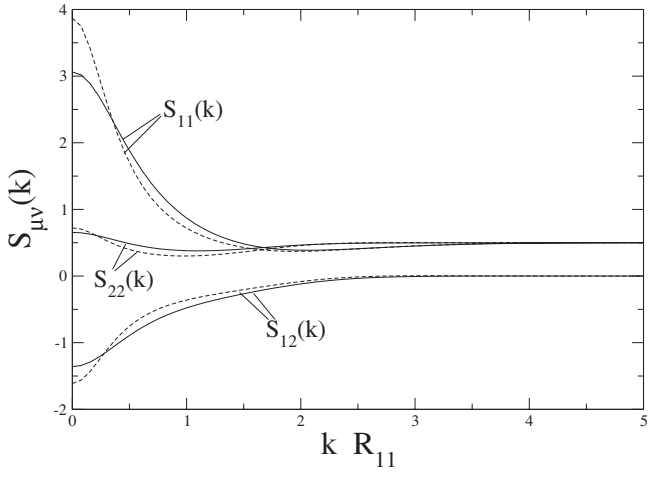

Fig. 10. HNC partial structure factors for the non-symmetric system $R_{11} = 1.0$, $R_{12} = 1.582$, $R_{22} = 2.0$, $\epsilon^*_{11} = \epsilon^*_{12} = \epsilon^*_{22} = 2.0$, $\rho R^3_{11} = 0.188$, $x = 0.5$. The solid lines represent the HNC results, the dashed lines the RPA partial structure factors. The enhanced values at $k = 0$ show that this system is close to the spinodal.

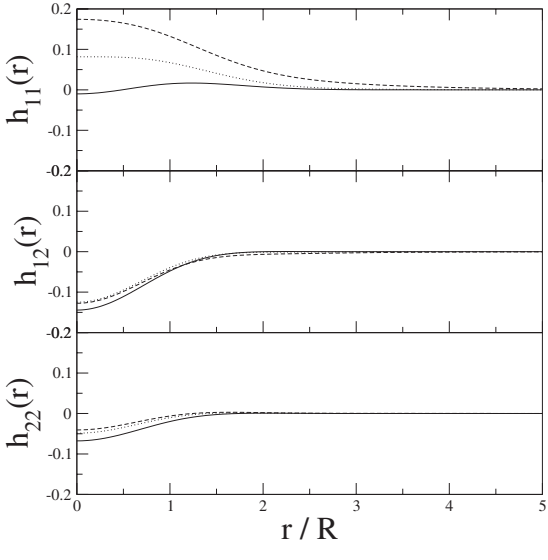

Fig. 11. HNC pair correlation functions of particles in the symmetric case with $\epsilon^*_{11} = \epsilon^*_{22} = 0.1$, $\epsilon^*_{12} = 0.2$, at a concentration $x = 0.9$ and densities below the binodal ($\rho R^3 = 2.0$, solid line), on the binodal ($\rho R^3 = 5.0$, dotted line) and near the spinodal ($\rho R^3 = 6.7$, dashed line). The results for the minority species 1 point towards clustering.

within the RPA, compared to the previously studied one-component case.[18] The peak in the structure factors at $k = 0$ as the spinodal is approached is expected, as explained earlier. More surprising perhaps is the appearance of peaks in the pair correlation functions as $r \to 0$, or at finite r. Peaks at $r \to 0$ are of course precluded in the presence of hard cores, but are quite significant in the present penetrable core model and point to a novel physical mechanism to trigger phase separation, namely the clustering of the minority species, as observed, e.g., in Fig. 11 for the symmetric case. The clustering can be explained by a simple "energetic" argument: the particles of the majority species tend to maximise their mutual distances. If the repulsion between unlike particles is stronger than between like ones, particles of the minority species prefer to cluster in the voids left by the majority species, rather than overlap with particles of the latter. This mechanism drives phase separation.

6. CONCLUSION

The two-component extension of the gaussian core model leads to non-trivial phase behaviour, which we have investigated within RPA and HNC theories. The former is partially analytic, while the latter requires only a modest numerical effort to calculate partial pair correlation functions and the resulting thermodynamic properties. While the pair structure shows some unexpected features, the most interesting prediction is the occurrence of phase separation induced by purely repulsive pair interactions. As expected for this model of penetrable particles, phase separation is driven by an enhanced repulsion between unlike particles compared to the like-particle interaction.

A special feature of the GCM mixtures is that at high densities of both species, the mixture behaves like a "mean field fluid," i.e., the RPA becomes asymptotically exact.[17, 18] This means that at finite densities, the RPA makes semi-quantitavely valid predictions for the phase behaviour, and allows a rapid exploration of potential parameter space to search for likely conditions for phase separation.

The nature of the link between the behaviour of the binary GCM and that of a binary polymer solution must still be worked out in detail, mainly because the effective interactions between the centres of mass of the polymer coils are state-dependent.[13] For a one-component system at lower densities, the structure is not very sensitive to the state-dependence.[29, 30] We therefore expect the binary GCM to make qualitatively correct predictions for the structure of binary polymer solutions in the dilute and beginning of the semi-dilute regimes. The link to the phase-behaviour is less clear. Because the GCM uses a fixed potential, it is mainly relevant to

behaviour in the dilute regime. While polymers in a melt are known to phase-separate rather easily,[2] in the dilute regime for good solvents they are not expected to phase-separate.[3] This appears to be confirmed by the results shown in Fig. 2. However, it may be that for poorer solvent, or for stronger polymer incompatibilities, a regime where the polymers phase-separate at low densities could open up. If this is the case, then the binary GCM would be a useful coarse-grained model with which one could rapidly explore the qualitative phase behaviour of this regime.

Another open question relates to the critical behaviour of the binary GCM in the immediate vicinity of the critical consolute point. The RPA clearly predicts mean field exponents. As regards the exact exponents, it is not obvious whether the correct critical behaviour of the model necessarily belongs to the Ising universality class, since there is no clear correspondence between GCM mixtures and standard lattice models, due to the penetrability of the particles. The question of the correct universality class, a subject dear to the heart of Michael Fisher, must be considered as open.

APPENDIX A: SOLUTION OF THE VIRIAL ROUTE IN RPA

We consider the GCM where the potentials have equal range $R_{11} = R_{12} = R_{22} = R$, and the heights of the repulsion potentials of like particles are the same for both species $\epsilon_{11} = \epsilon_{22}$. Without loss of generality we can set $V_{11} = 1$. Then we have

$$\hat{c}_{\mu\nu}(k) = -V_{\mu\nu} e^{-k^2R^2/4}, \tag{A1}$$

with

$$V_{\mu\nu} = \epsilon^*_{\mu\nu} R^3. \tag{A2}$$

If we introduce the abbreviation $\hat{z}(k) \equiv \rho V_{11} e^{-k^2R^2/4}$ and set $\Delta V = V_{12}^2 - V_{11}^2 = V_{12}^2 - 1$, the OZ Eq. (6) reduce to (using Eq. (7)):

$$\rho\hat{h}_{11}(k) = \frac{x_2\,\Delta V\hat{z}(k)^2 - \hat{z}(k)}{\Delta(k)} \tag{A3a}$$

$$\rho\hat{h}_{12}(k) = -\frac{V_{12}\hat{z}(k)}{\Delta(k)} \tag{A3b}$$

$$\rho\hat{h}_{22}(k) = \frac{x_1\Delta V\hat{z}(k)^2 - \hat{z}(k)}{\Delta(k)} \tag{A3c}$$

$$\Delta(k) = 1 + \hat{z}(k) - x(1-x)\,\Delta V\hat{z}(k)^2 \tag{A3d}$$

The denominator $\Delta(k)$ in Eq. (6) has the zeros

$$z_1 = \frac{1+\sqrt{1+4x(1-x)\,\Delta V}}{2x(1-x)\,\Delta V} > 0 \tag{A4a}$$

$$z_2 = \frac{1-\sqrt{1+4x(1-x)\,\Delta V}}{2x(1-x)\,\Delta V} < 0 \tag{A4b}$$

The positive root z_1 is the spinodal density at any given composition.

The virial Eq. (13) gives

$$\frac{\beta P^{\mathrm{V}}}{\rho} - \frac{\beta P^{\mathrm{C}}}{\rho} = -\frac{2\pi}{3}\rho \sum_{\mu}\sum_{\nu} x_\mu x_\nu \int_0^\infty r^3 \frac{d\beta v_{\mu\nu}(r)}{dr} h_{\mu\nu}(r)\, dr \tag{A5a}$$

$$= \frac{1}{3}\rho \sum_{\mu}\sum_{\nu} x_\mu x_\nu \int d\mathbf{r}\, \epsilon_{\mu\nu}(r^2/R^2)\, e^{-r^2/R^2} h_{\mu\nu}(r). \tag{A5b}$$

Evaluating this integral in Fourier space and making use of the Parseval theorem leads to

$$\frac{\beta P^{\mathrm{V}}}{\rho} - \frac{\beta P^{\mathrm{C}}}{\rho} = \frac{1}{3}\rho \sum_{\mu}\sum_{\nu} x_\mu x_\nu \int d\mathbf{k}\, V_{\mu\nu} \left[\frac{3}{2} - \frac{k^2R^2}{4}\right] e^{-r^2/R^2} \hat{h}_{\mu\nu}(k)$$

$$= \frac{1}{12}\int d\mathbf{k}\, \frac{\hat{z}(k)^2}{\Delta(k)} [x_1x_2\hat{z}(k)\,\Delta V - 2x_1x_2\Delta V - 1][6 - k^2R^2] \tag{A6}$$

This integral cannot be evaluated analytically in general. However, if the density is below the spinodal density for a given composition, one can expand the denominator in the integrand in a power series with respect to $\hat{z}(k)$. The integral can then be evaluated term by term, interchanging the integration and the summation. In order to make the symmetry between the two species explicit, we write $x = \frac{1+\xi}{2}$. The shifted concentration ξ now varies between -1 and 1, with $\xi = 0$ corresponding to $x = 0.5$.

With the definition of the polylogarithmic function

$$\mathrm{Li}_\alpha(x) = \sum_{n=1}^{\infty} \frac{x^n}{n^\alpha}, \tag{A7}$$

and the auxiliary function

$$\aleph(\alpha) = \frac{1}{2\alpha}[\mathrm{Li}_{3/2}(-\alpha) - \mathrm{Li}_{5/2}(-\alpha)] \tag{A8}$$

evaluation of (A6) leads to

$$\begin{aligned}\frac{\beta P}{\rho} = 1 &+ \frac{1}{4}\rho[1+V_{12}-\xi^2\,\Delta V] \\ &- \frac{z_2(1-\xi^2)\,\Delta V}{4\pi^{3/2}R^3}\,\aleph\left(-\frac{\rho}{z_1}\right) \\ &- \frac{z_1(1-\xi^2)\,\Delta V}{4\pi^{3/2}R^3}\,\aleph\left(-\frac{\rho}{z_2}\right).\end{aligned} \tag{A9}$$

This can be integrated to give the free energy per particle

$$\begin{aligned}\beta f(x,\rho) = f^{\mathrm{id}} &+ f^{\mathrm{mix}}(x) \\ &+ \frac{1}{4}\rho[1+V_{12}-\xi^2\Delta V] \\ &+ \frac{1}{2\pi^{3/2}\rho R^3}\left[\mathrm{Li}_{5/2}\,(\rho/z_1)+\mathrm{Li}_{5/2}\,(\rho/z_2)+\rho\right]\end{aligned} \tag{A10}$$

From that we get the chemical potentials as

$$\begin{aligned}\beta\mu_1 = \log(\Lambda^3\rho) &+ \log\left(\frac{1-\xi}{2}\right) + \frac{1-\xi}{2}\rho + V_{12}\,\frac{1+\xi}{2}\rho + \frac{1}{2\pi^{3/2}R^3} \\ &+ \frac{1}{2\pi^{3/2}R^3(1-\xi)\,\rho}\,\mathrm{Li}_{3/2}\left(\frac{\rho}{z_1}\right)\left[1+\frac{\xi}{\sqrt{1+\Delta V(1-\xi^2)}}\right] \\ &+ \frac{1}{2\pi^{3/2}R^3(1-\xi)\,\rho}\,\mathrm{Li}_{3/2}\left(\frac{\rho}{z_2}\right)\left[1-\frac{\xi}{\sqrt{1+\Delta V(1-\xi^2)}}\right],\end{aligned} \tag{A11}$$

$$\begin{aligned}\beta\mu_2 = \log(\Lambda^3\rho) &+ \log\left(\frac{1+\xi}{2}\right) + \frac{1+\xi}{2}\rho + V_{12}\,\frac{1-\xi}{2}\rho + \frac{1}{2\pi^{3/2}R^3} \\ &+ \frac{1}{2\pi^{3/2}R^3(1+\xi)\,\rho}\,\mathrm{Li}_{3/2}\left(\frac{\rho}{z_1}\right)\left[1-\frac{\xi}{\sqrt{1+\Delta V(1-\xi^2)}}\right] \\ &+ \frac{1}{2\pi^{3/2}R^3(1+\xi)\,\rho}\,\mathrm{Li}_{3/2}\left(\frac{\rho}{z_2}\right)\left[1+\frac{\xi}{\sqrt{1+\Delta V(1-\xi^2)}}\right].\end{aligned} \tag{A12}$$

It is easily checked that $\mu_1(\xi,\rho)=\mu_2(-\xi,\rho)$, due to the symmetry of the model. Note that these expressions become singular when $\rho \geqslant z_1 \equiv \rho_s$. This is a mathematical artefact originating in the interchange of summation and integration in (A6), which renders the expressions for P and μ unusable for binodal calculations.

APPENDIX B: ANALYTIC SOLUTION OF THE RPA-C BINODAL IN THE SYMMETRIC CASE

The phase diagram simplifies considerably in the symmetric case where $V_{11} = V_{22}$. We express V_{12} as $V_{12} = V_{11}(1+\gamma)$ and note that demixing occurs when the dimensionless parameter γ is positive. As above we introduce the reduced quantities $\rho^* = \rho V_{11}$ and $P^* = \beta P V_{11}$. Because of the symmetry of the problem, all quantities must be invariant with respect to the transformation $\rho \to \rho$, $x \to 1-x$, $1 \leftrightarrow 2$, which corresponds to a relabeling of species 1 and 2. As in Appendix A, we make use of the shifted concentration ξ to make this symmetry explicit. The pressure and the chemical potentials can now be expressed in terms of the variables ρ^* and ξ:

$$P^* = \rho^* + \frac{1}{4}\rho^{*2}(2+\gamma) - \frac{1}{4}\rho^{*2}\gamma\xi^2 \tag{B1a}$$

$$\beta\mu_1 = \ln(\rho^*) + \ln\left(\frac{1-\xi}{2}\right) + \frac{1}{2}\rho^*(2+\gamma) + \frac{1}{2}\rho^*\xi\gamma \tag{B1b}$$

$$\beta\mu_2 = \ln(\rho^*) + \ln\left(\frac{1+\xi}{2}\right) + \frac{1}{2}\rho^*(2+\gamma) - \frac{1}{2}\rho^*\xi\gamma \tag{B1c}$$

In these equations we have set $\Lambda = V_{11}$, which merely shifts the free energy per particle by a constant amount and thus does not change the phase diagram.

Two coexisting phases α, β must have the same pressure and chemical potentials, respectively:

$$P^\alpha = P^\beta, \qquad \mu_1^\alpha = \mu_1^\beta, \qquad \mu_2^\alpha = \mu_2^\beta \tag{B2}$$

Because of the symmetry in this model, coexisting phases must have the same density $\rho^\alpha = \rho^\beta$ and the corresponding concentrations must fulfill $x^\alpha = 1 - x^\beta$. Considering this, equal pressure in both phases is trivially fulfilled, and the two conditions of equal chemical potentials become equivalent. The relation between the binodal density ρ_b and concentration is

$$\rho^*_b = \frac{1}{\gamma\xi}\ln\left(\frac{1+\xi}{1-\xi}\right). \tag{B3}$$

Expanding the binodal densities around the critical point gives

$$\rho^*_b = \frac{2}{\gamma}\left[1 + \frac{1}{3}\xi^2 + \mathcal{O}(\xi^4)\right]. \tag{B4}$$

From the series expansions we see that for all $\gamma > 0$ the spinodal lies inside the binodal. Within the RPA approximation we thus get an analytically exact solution for a fluid-fluid demixing transition of a liquid consisting of purely repulsive particles. As expected in this treatment, the resulting critical exponents are mean-field exponents.

ACKNOWLEDGMENTS

R. Finken is indebted to the Oppenheimer Fund for their support. A. A. Louis would like to thank the Isaac Newton Trust, Cambridge, for funding.

REFERENCES

1. J. S. Rowlinson and F. Swinton, *Liquids and Liquid Mixtures*, 3rd edn. (Butterworths, London, 1982).
2. M. Doi, *Introduction to Polymer Physics* (Oxford University Press, Oxford, 1995).
3. D. Broseta, L. Leibler, and J.-F. Joanny, *Macromolecules* **20**:1935 (1987).
4. J. S. van Duijneveldt, A. W. Heinen, and H. N. W. Lekkerkerker, *Europhys. Lett.* **21**:369 (1993); A. D. Dinsmore, A. G. Yodh, and D. J. Pine, *Phys. Rev. E* **52**:4045 (1995); A. Imhof and J. K. G. Dhont, *Phys. Rev. Lett.* **75**:1662 (1995).
5. S. M. Ilett, A. Orrock, W. C. K. Poon, and P. N. Pusey, *Phys. Rev. E* **51**:1344 (1995).
6. S. Asakura and F. Oosawa, *J. Polym. Sci., Polym. Symp.* **33**:183 (1958); A. Vrij, *Pure Appl. Chem.* **48**:471 (1976).
7. T. Biben and J. P. Hansen, *Phys. Rev. Lett.* **66**:2215 (1991); *J. Phys. Cond. Matt.* **3**:F65 (1991).
8. M. Dijkstra, R. van Roij, and R. Evans, *Phys. Rev. E* **59**:5744 (1999).
9. A. A. Louis, R. Finken, and J. P. Hansen, *Phys. Rev. E* **61**:R1028 (2000).
10. A. Y. Grosberg, P. G. Khalatur, and A. R. Khoklov, *Makromol. Chem.* **3**:709 (1982).
11. B. Krüger, L. Schäfer, and A. Baumgärtner, *J. Phys. (Paris)* **50**:319 (1989).
12. J. Dautenhahn and C. K. Hall, *Macromolecules* **27**:5399 (1994).
13. A. A. Louis, P. G. Bolhuis, J. P. Hansen, and E. J. Meijer, *Phys. Rev. Lett.* **85**:2522 (2000); P. G. Bolhuis, A. A. Louis, J. P. Hansen, and E. J. Meijer, *J. Chem. Phys.* **114**:4296 (2001).
14. T. A. Witten and P. A. Pincus, *Macromolecules* **19**:2509 (1986); C. N. Likos, H. Löwen, M. Watzlawek, B. Abbas, O. Jucknischke, J. Allgauer, and D. Richter, *Phys. Rev. Lett.* **80**:4450 (1998).
15. C. N. Likos, M. Schmidt, H. Löwen, M. Ballauff, D. Pötschke, and P. Lindner, *Macromolecules* **34**:2914 (2000).
16. C. N. Likos, M. Watzlawek, and H. Löwen, *Phys. Rev. E* **58**:3135 (1998).
17. A. Lang, C. N. Likos, M. Watzlawek, and H. Löwen, *J. Phys. Cond. Matter* **12**:5087 (2000), C. N. Likos, A. Lang, M. Watzlawek, and H. Löwen, *Phys. Rev. E* **63**:1206 (2001).
18. A. A. Louis, P. G. Bolhuis, and J. P. Hansen, *Phys. Rev. E* **62**:7961 (2000).
19. A. J. Archer and R. Evans, *Phys. Rev. E* **64**:41501 (2001).
20. F. H. Stillinger, *J. Chem. Phys.* **65**:3968 (1976).
21. See, e.g., S. N. Lai and M. E. Fisher, *Mol. Phys.* **88**:1373 (1996).
22. P. J. Hoogerbrugge and J. M. V. A. Koelman, *Europhys. Lett.* **19**:155 (1992).

23. R. D. Groot and P. B. Warren, *J. Chem. Phys.* **107**:4423 (1997).
24. C. M. Wijmans, B. Smit, and R. D. Groot, *J. Chem. Phys.* **114**:7644 (2001).
25. See, e.g., J. P. Hansen and I. R. McDonald, *Theory of Simple Liquids*, 2nd edn. (Academic Press, London, 1986).
26. L. Verlet and D. Levesque, *Physica* **28**:1124 (1962).
27. L. Belloni, *J. Chem. Phys.* **98**:8080 (1993).
28. S. Fishman and M. E. Fisher, *Physica A* **108**:1 (1981).
29. P. G. Bolhuis, A. A. Louis, and J.-P. Hansen, *Phys. Rev. E* **64**:021801 (2001).
30. P. G. Bolhuis and A. A. Louis, *Macromolecules* **35**:1860 (2002).